Journal of Magnetic Resonance 196 (2009) 133–141

Contents lists available at ScienceDirect

Journal of Magnetic Resonance

journal homepage: www.elsevier.com/locate/jmr

Fast acquisition of multi-dimensional spectra in solid-state NMR enabled by ultra-fast MAS

Ségolène Laage [a], Joseph R. Sachleben [b], Stefan Steuernagel [c], Roberta Pierattelli [d], Guido Pintacuda [a], Lyndon Emsley [a,*]

[a] Université de Lyon, CNRS/ENS Lyon/UCB-Lyon 1, Centre RMN à Très Hauts Champs, 5 rue de la Doua, 69100 Villeurbanne, France
[b] Otterbein College, Columbus, OH, USA
[c] Bruker Biospin, Karlsruhe, Germany
[d] Department of Chemistry and Magnetic Resonance Center (CERM), University of Florence, Via Luigi Sacconi 6, 50019 Sesto Fiorentino (Firenze), Italy

ARTICLE INFO

Article history:
Received 20 June 2008
Revised 29 October 2008
Available online 7 November 2008

Keywords:
Magic angle spinning
NMR
Proteins
Low power

ABSTRACT

The advantages offered by ultra-fast (>60 kHz) magic angle spinning (MAS) rotation for the study of biological samples, notably containing paramagnetic centers are explored.

It is shown that optimal conditions for performing solid-state ^{13}C NMR under 60 kHz MAS are obtained with low-power CW ^{1}H decoupling, as well as after a low-power ^{1}H,^{13}C cross-polarization step at a double-quantum matching condition. Acquisition with low-power decoupling highlights the existence of rotational decoupling sidebands. The sideband intensities and the existence of first and second rotary conditions are explained in the framework of the Floquet–van Vleck theory.

As a result, optimal ^{13}C spectra of the oxidized, paramagnetic form of human copper zinc superoxide dismutase (SOD) can be obtained employing rf-fields which do not exceed 40 kHz during the whole experiment. This enables the removal of unwanted heating which can lead to deterioration of the sample. Furthermore, combined with the short ^{1}H T_1s, this allows the repetition rate of the experiments to be shortened from 3 s to 500 ms, thus compensating for the sensitivity loss due to the smaller sample volume in a 1.3 mm rotor. The result is that 2D ^{13}C–^{13}C correlation could be acquired in about 24 h on less than 1 mg of SOD sample.

1. Introduction

Interest in solid-state NMR (SSNMR) as a tool for studying the structure and dynamics of biological molecules has considerably grown during the last decades [1–6]. The past 10 years have notably witnessed a remarkable development in magic angle spinning (MAS) probe technology, which has enabled a considerable increase in sample spinning and decoupling frequencies, allowing stronger dipolar couplings to be averaged better and better. For instance, the size of commercially available rotors has progressively decreased, and the range of attainable spinning frequencies has correspondingly increased. Rotation frequencies have gone from the so-called fast (20 kHz) and very-fast (35 kHz) regimes to the actual "ultra-fast" regime of more than 60 kHz, reached using commercial 1.3 mm rotors. This frequency exceeds the strength of homonuclear protons dipolar coupling and is therefore expected to enter a new regime for spin dynamics [7].

One of the first noticeable effects offered by high spinning frequencies was the gain in resolution. For example, it was observed experimentally that the linewidth in uniformly ^{13}C labeled compounds decreases at faster MAS rates [8]. The increase in sensitivity is particularly striking in the case of paramagnetic nuclei [9–11] or quadrupolar nuclei [12]. More recently, ultra-fast MAS applications have notably enabled the recording of indirect detection of heteronuclei through ^{1}H NMR signals in ^{15}N [13] and ^{13}C experiments [14,15].

A key advantage often intuitively connected to the use of small rotor sizes is the possibility to apply stronger irradiation fields, since smaller rf coils and sample volumes significantly increase the nutation frequencies for a given rf power applied to the probe coil. In solid-state NMR experiments, the size of the anisotropic interactions is usually not much smaller than the rf-field used to modulate them, and this often results in incomplete averaging. Large rf-fields would then be beneficial particularly for experiments that use dipolar and quadrupolar decoupling, recoupling, or broadband single and multiple quantum excitation.

However, it may be more interesting to note that ultra-fast MAS opens new perspectives for techniques which make use of *low-power irradiation*. Meier and co-workers have indeed demonstrated the use of low-power decoupling at high-frequency MAS

* Corresponding author. Fax: +33 4 72 72 88 60.
E-mail address: lyndom.emsley@ens-lyon.fr (L. Emsley).

1090-7807/$ - see front matter © 2008 Elsevier Inc. All rights reserved.
doi:10.1016/j.jmr.2008.10.019

in order to achieve heteronuclear spin decoupling [8]. Using average Hamiltonian theory, they showed the advantage of inversing the averaging processes ($\omega_1^H < \omega_r$) compared to the normal high-power approach. They demonstrated this with XiX decoupling [16] and then proved its applicability for the decapeptide antamanide at 60 kHz MAS [7]. Kotecha et al. recently compared the efficiency of different decoupling sequences at high spinning speeds depending on the multiplicity of the carbon under consideration in ubiquitin samples [17]. Griffin et al. have also recently discussed the use of low-load decoupling during spin-echo experiments [18]. Low-field decoupling is thus an important alternative, in particular for the study of biological substrates with high dielectric constants, where prolonged high-power irradiations can lead to undesired, often disastrous, heating of the sample.

In the following, we provide an analysis of effects of fast MAS on both decoupling and cross-polarization. This analysis will summarize results that were already partially presented. For example, Meier studied the effect of fast MAS on cross-polarization and proved the possibility of double-quantum Hartmann–Hahn matching [19]. A theoretical analysis of CPMAS using Floquet theory as well as simulations were then developed by Vega [20,21]. As for decoupling, several theoretical studies using Floquet theory and van Vleck transformation were carried out by Sachleben [22,23], Griffin and co-workers [24], Meier and co-workers [25] and Vega and co-workers [26]. All these results will be recast here using Floquet–van Vleck theory. We will then highlight how the improved partial averaging of the homonuclear hamiltonian by very-fast sample rotation affects the cross-polarization and heterodecoupling processes. These effects are examined and explained in a simple model compound, 2-(^{13}C)-L-alanine, as well as in copper(II), zinc(II)-superoxide dismutase (SOD), a paramagnetic protein of 32 kDa.

2. Experimental section

All experiments were performed on a Bruker Avance III spectrometer operating at a proton frequency of 500 MHz, and equipped with a double-resonance 1.3 mm CP-MAS probe.

Purified ^{13}C, ^{15}N-labeled, stabilized copper(II), zinc(II)-superoxide dismutase was obtained from ProtEra srl (Sesto Fiorentino, Italy). A microcrystalline crystallized sample was prepared as previously described [27], and directly centrifuged into the NMR rotor.

RF-field strengths were determined by recording ^{1}H and ^{13}C nutation curves. Other experimental details are given in the figure captions for each spectrum.

3. Theory

3.1. Cross-polarization during fast MAS

CP under MAS has been extensively studied in the past [28,29]. Meier studied the effect of fast MAS on cross-polarization and proved the possibility of double-quantum Hartmann–Hahn matching [19]. A theoretical analysis of CPMAS using Floquet theory as well as simulations was then developed by Vega and co-workers [20,21]. In the following, we will provide a summary of these results.

In the framework of Floquet theory, the most general case of a rotating $I_N S(1/2)$ spin system is represented by the Hamiltonian:

$$\mathrm{H} = -\omega_1^S S_Z - \omega_1^I I_Z + \omega_r R_{Z'} + \mathrm{H}_{IS} + \mathrm{H}_{II}. \tag{1}$$

This Hamiltonian is written in a mixed quantization frame where I- and S-spins are quantized along their respective rf-fields, with rf-field strengths of ω_1^I and ω_1^S, respectively, and the rotation of the sample (at a frequency ω_r) is quantized along the rotor axis. The rotational quantum number operator, $R_{Z'}$, measures the deviation of the angular momentum from its average value about the rotation axis. If the rotor state is defined by the ket, $|n\rangle$, where n is the number of rotor quanta in that state, then $|n\rangle$ is an eigenstate of $R_{Z'}$, defined by the eigenvalue equation

$$R_{Z'}|n\rangle = n|n\rangle. \tag{2}$$

The operators F_p are the p rotor quantum raising and lowering operators defined by

$$F_p|n\rangle = |n+p\rangle. \tag{3}$$

These Floquet operators follow the commutation relations

$$[F_m, F_n] = 0 \tag{4}$$

and

$$[R_{Z'}, F_n] = nF_n. \tag{5}$$

In this way, when the two irradiation fields are applied, the $I_N S$ system can be represented by two basis manifolds of Floquet states $\{|M,\alpha,n\rangle,|M,\beta,n\rangle\}$, where $|M\rangle$ is one of the $\frac{N!}{(N-(M+N/2))!(M+N/2)!}$ coupled I-spin product functions with total spin number M, n is assumed to take values from $-\infty$ to ∞, and $|\alpha\rangle$ and $|\beta\rangle$ are the eigenstates of the S spin. The energy of these manifolds are, respectively, $-M\omega_1^I - \frac{1}{2}\omega_1^S + n\omega_r$ and $-M\omega_1^I + \frac{1}{2}\omega_1^S + n\omega_r$. This is illustrated in Fig. 1.

In this formalism, the homonuclear coupling can be expressed as:

$$\mathrm{H}_{II} = -\frac{1}{2}\sum_{ij}\sum_{p=-2}^{2}\omega_{ij}^{(p,0)}T_{2,0}^{(ij)}F_p + \sqrt{\frac{3}{8}}\sum_{ij}\sum_{p=-2}^{p}\omega_{ij}^{(p,0)}(T_{2,2}^{(ij)} + T_{2,-2}^{(ij)})F_p \tag{6}$$

where

$$\omega_{ij}^{(p,0)} = \omega_{ij}D_{0,p}^{(2)}(\alpha_{ij},\beta_{ij},\gamma_{ij})D_{0,p}^{(2)}(0,\beta_r,0). \tag{7}$$

$\omega_{ij} = -\hbar\gamma_I^2/r_{ij}^3$ is the proton–proton dipolar coupling constant, and the $D_{m,n}^{(2)}(\Omega)$ are the second rank Wigner rotation matrix elements that rotate from the principle axis system of the homonuclear coupling to the rotor axis system, for $\Omega_{ij} = (\alpha_{ij},\beta_{ij},\gamma_{ij})$, and from the rotor axis system to the laboratory, $\Omega = (0,\beta_r,0)$. This term removes the degeneracies between the Floquet manifolds of states, and creates a band of mixed states that exhibit an energy spread of the order of $|\omega_{ij}|^3/\omega_r^2$.

The heteronuclear part of this Hamiltonian can be rewritten in terms of raising and lowering operators as

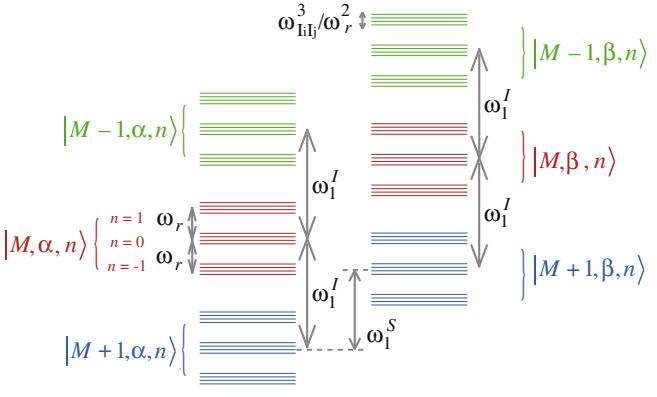

Fig. 1. Schematic representation of the Floquet energy states in the tilted rotating frame of a $I_N S$ spin system under MAS.

$$H_{IS} = -\sum_{i=1}^{N}\sum_{p=-2}^{2}\omega_{I_iS}^{(p,0)} 2I_{iX}S_X F_p$$
$$= -\frac{1}{2}\sum_{i=1}^{N}\sum_{p=-2}^{2}\omega_{I_iS}^{(p,0)}(I_{i,+}S_+ + I_{i,-}S_-)F_p - \frac{1}{2}\sum_{i=1}^{N} \times \sum_{p=-2}^{2}\omega_{I_iS}^{(p,0)}(I_{i,+}S_- + I_{i,-}S_+)F_p \quad (8)$$

where

$$\omega_{I_iS}^{(p,0)} = \omega_{IS} D_{0,p}^{(2)}(\alpha_i,\beta_i,\gamma_i) D_{0,p}^{(2)}(0,\beta_r,0). \quad (9)$$

and $\omega_{IS} = -\hbar\gamma_I\gamma_S/r_{IS}^3$ is the heteronuclear dipolar coupling.

The heteronuclear coupling gives rise to both double- and zero-quantum terms both of which can lead to cross-polarization [19,20]. For the zero-quantum case, this can be seen by noticing that when $\omega_1^S - \omega_1^I = p\omega_r$ (for $p = \pm 1, \pm 2$), the zero-quantum heteronuclear term

$$H_{ZQCP} = -\frac{1}{2}\omega_{IS}^{(p,0)}(I_{i,+}S_- F_{-p} + I_{i,-}S_+ F_p), \quad (10)$$

commutes with rf and rotation parts of the Hamiltonian,

$$H_0 = -\omega_1^S S_Z - \omega_1^I I_Z + \omega_r R_{Z'}. \quad (11)$$

This thus couples the $|M,\alpha,n\rangle$ and $|M+1,\beta,n+k\rangle$ manifolds with $p = \pm 1, \pm 2$, allowing the term in Eq. (10) to drive zero-quantum cross-polarization. Similarly, the term

$$H_{DQCP} = -\frac{1}{2}\omega_{IS}^{(p,0)}(I_+S_+F_{-p} + I_-S_-F_p) \quad (12)$$

will cause double-quantum cross-polarization between the $|M,\alpha,n\rangle$ and $|M-1,\beta,n+k\rangle$ manifolds when their energies $E_\alpha^M(n)$ and $E_\beta^M(n)$ are about equal, that is for $\omega_1^I + \omega_1^S = p\omega_r$ with $p = \pm 1, \pm 2$.

Cross-polarization under MAS can thus theoretically occur through two kinds of mechanisms: one involves the zero-quantum part of the heteronuclear dipolar coupling whereas the other one relies on the double-quantum part of the same interaction.

Further analysis using quasi-equilibrium (QE) spin thermodynamics allows us to determine the maximum polarization achievable for ZQ- and DQCP under fast MAS. Such an analysis is provided in Appendix A. It notably shows that DQCP will lead to negative enhancements as compared to ZQ processes. The analysis predicts that the maximum polarization achievable is the same for equivalent conditions.

In conclusion, if the CP matching curve under ultra-fast MAS is measured, ZQCP is expected to give rise to a series of strong positively phased peaks spaced by $\pm p\omega_r$ about the normal Hartmann–Hahn condition of $\omega_1^I = \omega_1^S$. In addition, strong, negatively phased peaks will appear at $\omega_1^I = p\omega_r - \omega_1^S$ due to DQCP.

3.2. Decoupling during fast MAS

Several theoretical studies of heteronuclear decoupling have been done using Floquet theory, and van Vleck transformation were used in this context by several authors [22–26]. In the following, we will provide a summary of these results, recast here in a uniform Floquet–van Vleck formalism.

Most of the interesting decoupling effects at high spinning frequencies can be demonstrated in an I_2S system. The Hamiltonian for such a spin system undergoing heteronuclear decoupling and MAS is

$$H = -\omega_0^S S_Z - \omega_1^I I_Z + \omega_r R_{Z'} - \sum_{i=1}^{2}\sum_{p=-2}^{2}\omega_{IS}^{(p,0)}(I_{i+}S_Z + I_{i-}S_Z)F_p$$
$$-\frac{1}{2}\sum_{p=-2}^{2}\omega_{12}^{(p,0)}T_{2,0}^{(12)}F_p + \sqrt{\frac{3}{8}}\sum_{p=-2}^{2}\omega_{12}^{(p,0)}(T_{2,2}^{(12)} + T_{2,-2}^{(12)})F_p, \quad (13)$$

Here again the Hamiltonian is written in a mixed quantization axis system, where the S-spin is quantized along the normal laboratory rotating frame, and the I-spins are quantized along the decoupling field.

Using the Hamiltonian in Eq. (13) and the commutation relations of the spin operators and of Eqs. (4) and (5), Floquet–van Vleck theory can be used to calculate the signal as a function of time. Far from rotary resonance, the signal has been shown to be [23]:

$$S(t) = \left\{1 - \frac{2}{5}\sum_{m=-2}^{2}(-1)^m \frac{\omega_{IS}^2}{(\omega_1^I + m\omega_r)^2} d_{m,0}^{(2)}(\beta_r) d_{-m,0}^{(2)}(\beta_r)\right\} e^{i\omega_0^S t} \quad \text{(centerband)}$$
$$+\frac{1}{5}\sum_{m=-2}^{2}(-1)^m \frac{\omega_{IS}^2}{(\omega_1^I + m\omega_r)^2} d_{m,0}^{(2)}(\beta_r) d_{-m,0}^{(2)}(\beta_r) e^{i(\omega_0^S + \omega_1^I + m\omega_r)t} \quad \text{(sidebands)}$$
$$+\frac{1}{5}\sum_{m=-2}^{2}(-1)^m \frac{\omega_{IS}^2}{(\omega_1^I - m\omega_r)^2} d_{m,0}^{(2)}(\beta_r) d_{-m,0}^{(2)}(\beta_r) e^{i(\omega_0^S - \omega_1^I + m\omega_r)t}. \quad \text{(sidebands)} \quad (14)$$

At a fixed rotation rate, Eq. (14) predicts a spectrum containing a strong peak at the isotropic frequency, ω_0^S, flanked by rotational decoupling sidebands at $\omega_0^S + \omega_1^I + m\omega_r$ and $\omega_0^S - \omega_1^I + m\omega_r$. The strongest of these is shifted from the isotropic frequency by $\pm(\omega_r - \omega_1^I)$. Rotary resonances occur when these rotational decoupling sidebands overlap the centerband, i.e. when $\omega_1^I = \omega_r$ or $\omega_1^I = 2\omega_r$. Notably, the existence of decoupling sidebands has already been predicted and experimentally observed [22]. In the presence of MAS, theory predicts that the decoupling sidebands break up into a set of rotational decoupling sidebands which, until now, have never been experimentally observed [23].

The interference of decoupling with MAS can therefore be summed up by two main results: the existence of rotational decoupling sidebands and a drastic loss of signal expected at rotary resonances.

4. Results and discussion

4.1. Cross-polarization during fast MAS

Fig. 2 shows the profiles of the C^α carbon signal in 2-(^{13}C)-L-alanine after a conventional CP experiment as a function of the proton rf-field strength, in which the carbon rf-field is kept constant at $\omega_1^C/2\pi = 160$ kHz (Fig. 2a) or $\omega_1^C/2\pi = 45$ kHz (Fig. 2b). The MAS frequency $\omega_r/2\pi$ was 68 kHz. The orders of the various matching conditions are labeled on the figure and correspond to both zero- and double-quantum cross-polarization conditions. Zero-quantum cross-polarization (ZQCP) occurs when $\omega_1^H - \omega_1^C = p\omega_r$ and give rise to peaks with positive intensity as illustrated in the theoretical section above. Double-quantum cross-polarization (DQCP) occurs when $\omega_1^H + \omega_1^C = p\omega_r$ and gives rise to peaks with negative intensity. Most importantly, we note that the CP efficiency obtained at the $p = 1$ DQCP condition in Fig. 2b with $\omega_1^C/2\pi = 45$ kHz and $\omega_1^H/2\pi = 23$ kHz is at least as great as any other available CP conditions at higher rf-fields.

In most CP studies until now, with spinning rates up to 30 kHz, the best CP transfers have always been obtained with high-power ^{1}H irradiation. Low-power schemes performed poorly in this regime, although fields of a few kHz should in principle be sufficient to lock ^{1}H and ^{13}C magnetization and drive the polarization transfer process. On the contrary, at the high rotation frequencies used in the experiments presented, comparable transfer efficiencies are found for the high-power regime and for the low-power $p = 1$ DQCP condition.

This phenomenon can be understood in the Floquet theory framework. At slow MAS, rotor states in different $|M,\alpha,n\rangle$ and

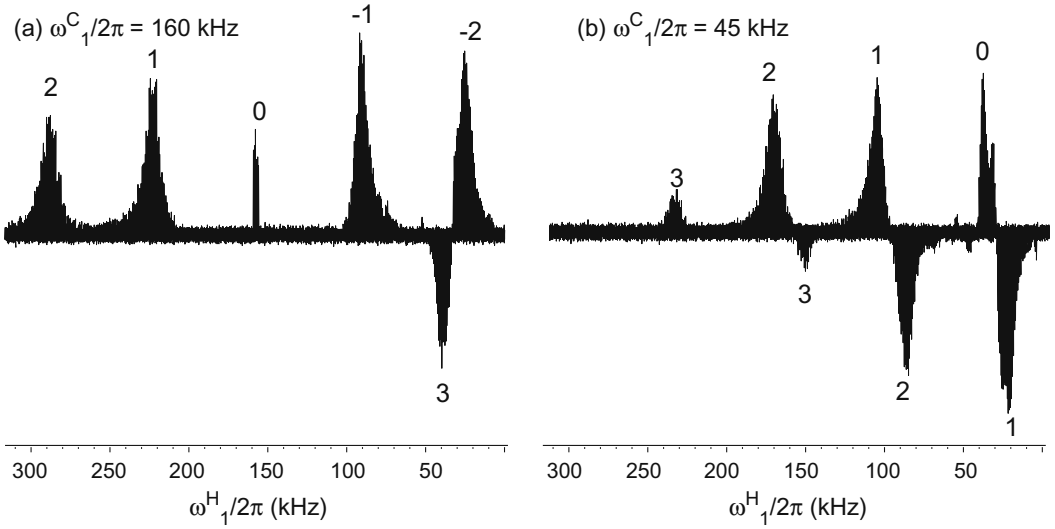

Fig. 2. ^{13}C CP profiles of 2-(^{13}C)-L-alanine at 68 kHz MAS. The intensity of the C$^{\alpha}$ carbon signal is monitored in a CP experiment (1 ms contact time) where the field strength $\omega_1^C/2\pi$ on the carbon channel is set to 160 kHz (a) or 45 kHz (b), and proton rf-field strength $\omega_1^H/2\pi$ is varied from 320 to 2 kHz.

$|M,\beta,n\rangle$ are matched as soon as ω_1^I and ω_1^S differ by integer multiples of ω_r to within the width of the manifolds, which is of the order of $|\omega_{ij}|^3/\omega_r^2$ (Fig. 3). Fig. 3a shows this for the classic case where the rf-fields are significantly larger that the rotor frequency. Only ZQ transitions are observed in the CP profile. Fig. 3b shows the CP profile expected when rf-fields are used with slow (here 10 kHz) spinning. In this case, overlapping ZQ and DQ transitions lead to partial cancellation of the transferred polarization (Fig. 3b), and the overall efficiency is reduced.

This behavior is substantially changed in the ultra-fast MAS regime. Here, first the width of the manifolds is substantially narrower (sharper Hartmann–Hahn matching) and, second, their spacing is substantially larger. As shown in Fig. 3c and d this allows overlap of ZQ and DQ transitions to be easily avoided for both high (3c) and low (3d) values of ω_1^I.

As a result, ultra-fast MAS rates allow efficient low-power CP experiments using low power on both channels, as verified by the experiments shown in Fig. 2. This situation is now reminiscent of the CP behavior observed at moderate spinning speeds on low-γ nuclei such as ^{15}N–^{13}C pairs [30].

4.2. Decoupling during fast MAS

Fig. 4 shows the intensity of the 2-(^{13}C)-L-alanine carbon signal under continuous wave (CW) heteronuclear decoupling as a function of the decoupling rf-field strength.

As notably discussed by Ernst et al. [8], three main phenomena contribute to the shape of this profile, namely the two $n = 1$ and $n = 2$ rotary resonances [31], clearly visible at $\nu_1^H = 60$ and 120 kHz, and the HORROR condition [32].

The terms in the Hamiltonian responsible for rotary resonance are

$$H^{RR} = -\omega_{IS}^{(-p,0)} I_{i+} S_Z F_p - \omega_{IS}^{(p,0)} I_{i-} S_Z F_{-p}, \quad (15)$$

where $p = 1$ or 2 and i labels the I-spin. Terms such as $I_{i-}S_ZF_{-p}$ cause the state of the ith I-spin to flip from the $|\frac{1}{2}\rangle \rightarrow |-\frac{1}{2}\rangle$ state while the rotor state decreases by p rotor quanta ($|n\rangle \rightarrow |n-p\rangle$). At the rotary resonance conditions described above, the energy levels connecting these transitions are degenerate and directly driven by the Hamiltonian terms given in Eq. (7). This recouples the heteronuclear dipolar interaction, leading to broadening of the S-spin resonance and thus to a dramatic loss of signal.

Homonuclear couplings have significant effects on rotary resonance. It has been shown theoretically [33], that the 1st and 2nd rotary resonances are partially quenched by the presence of homonuclear couplings. At high spinning frequencies, $\omega_r > \omega_{12}$, Eq. (13) is truncated by the rotation of the sample, $\omega_r R_{Z'}$, leading to reduction of the homonuclear part of the Hamiltonian. Under these conditions, the $n = 1$ and 2 rotary resonances are narrow and intense; however, in the low spinning regime, when $\omega_{12} > \omega_r$, the homonuclear coupling can truncate the terms that lead to rotary resonances in Eq. (15), and partially quench and broaden the rotary resonances.

The best decoupling over the whole range from 0 to 240 kHz is found here at ultra-fast MAS when $\nu_1^H = 24$ kHz, which corresponds roughly to $\frac{\nu_1^H}{\nu_r} = \frac{1}{2}$, that is the HORROR condition. At the HORROR condition, homonuclear dipolar couplings between ^{1}Hs are reintroduced [32,33], leading to partial removal of the heteronuclear coupling. This explains the improved decoupling observed under such conditions [33]. Interestingly, no evidence of improved decoupling at the HORROR condition is evident in similar profiles recorded under slow and moderate MAS rates, since in this regime the $n = 1$ and 2 rotary resonances are broader, and partially cancel the effect of the HORROR matching. In the slow spinning regime, the best overall decoupling is always found at the highest available power.

A more detailed analysis can be drawn from the spectra shown in Fig. 5, which presents a 2D array of CP/MAS carbon spectra of 2-(^{13}C)-L-alanine recorded under CW heteronuclear decoupling for different values of the decoupling rf-field, at 60 kHz MAS.

Here we observe the predicted first order rotational decoupling sidebands (at frequencies of $\omega_r - \omega_1^H$ and $-\omega_r + \omega_1^H$) which clearly appear in the range where $\omega_r < \omega_1^H < 2\omega_r$, as illustrated in Fig. 5c and d. As predicted, the rotational decoupling sidebands increase in intensity as they get closer to the centerband while the intensity of the centerband decreases. The centerband changes dramatically in the well known fashion when the rotary resonance is exactly matched (Fig. 5b). Second order rotational decoupling sidebands (at frequencies of $2\omega_r - \omega_1^H$ and $-2\omega_r + \omega_1^H$) are observed weakly at the approach to the second rotary resonance.

Decoupling sidebands have only been previously observed experimentally in liquid crystalline samples [22] and rotational decoupling sidebands have not been observed previously in solid samples undergoing MAS. This is probably because as predicted

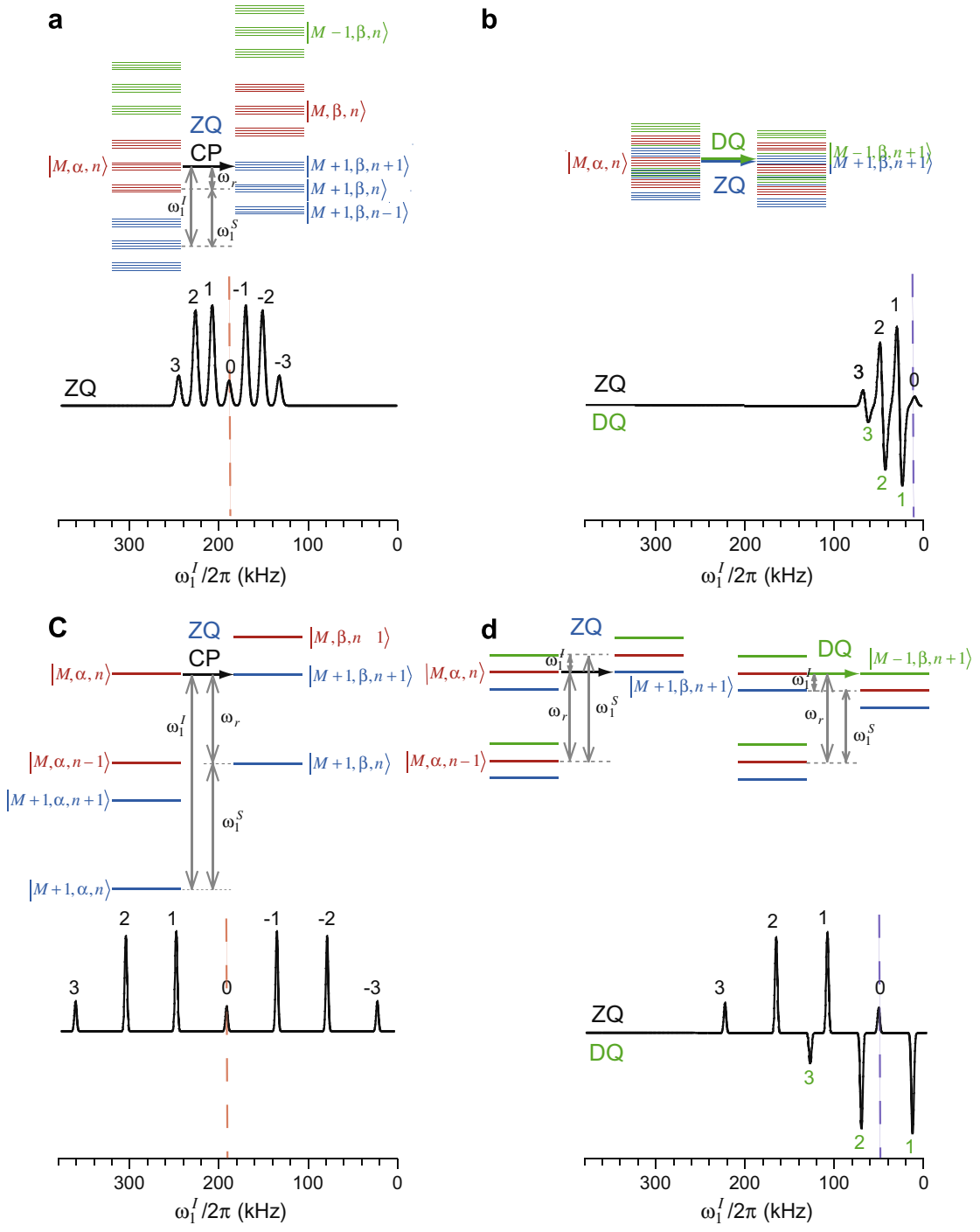

Fig. 3. Schematic explanation of cross-polarization occurring under low spinning speed (a and b) or ultra-fast MAS (c and d), at high irradiation fields (a and c) or low fields (b and d).

above, the sidebands narrow under fast MAS since their linewidths are determined by homo- and heteronuclear dipolar couplings. Better averaging of these dipolar couplings by fast MAS will reduce the width of the sidebands, making quite logical their observation for the first time here under ultra-fast MAS.

4.3. Application to fast acquisition of SSNMR spectra

Overall, the discussion above allows us to conclude that (i) efficient cross-polarization can be achieved at low rf power under ultra-fast MAS, and (ii) efficient decoupling can also be achieved with low rf-fields.

Fig. 6 confirms the effect of CW heteronuclear decoupling rf-field strengths on the CP/MAS carbon spectra of fully carbon-labeled SOD at 60 kHz MAS. Again, as illustrated in Fig. 6b and g, best resolution is obtained with low power decoupling ($\nu_1^H = 27$ kHz) as compared to decoupling at 110 kHz. As for the case of alanine, first order rotational decoupling sidebands of the aliphatic peak are observed at frequencies of $\omega_r - \omega_1^H$ and $-\omega_r + \omega_1^H$ (6a–d). They appear as broad resonances whose intensity increases on

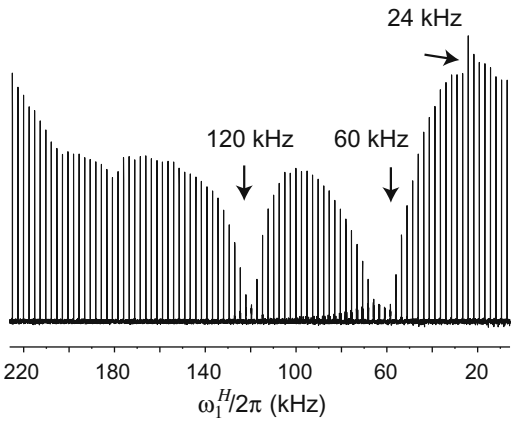

Fig. 4. Intensity of the ^{13}C resonance in 2-(^{13}C)-L-alanine in a CP experiment at 60 kHz MAS under CW ^{1}H decoupling, as a function of the decoupling rf-field strength.

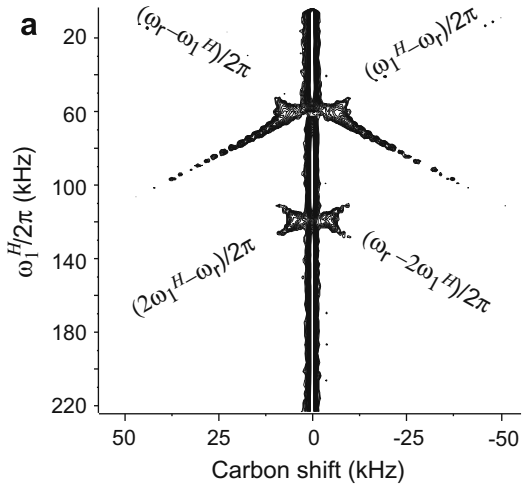

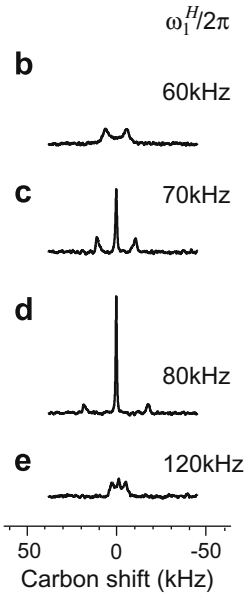

Fig. 5. (a) Array of CP/MAS carbon spectra of 2-(^{13}C)-L-alanine recorded at 60 kHz MAS under CW heteronuclear decoupling, with different values of the decoupling rf-field ω_1^H. Projections at different values of the decoupling rf-field ω_1^H, are shown in (b)–(e).

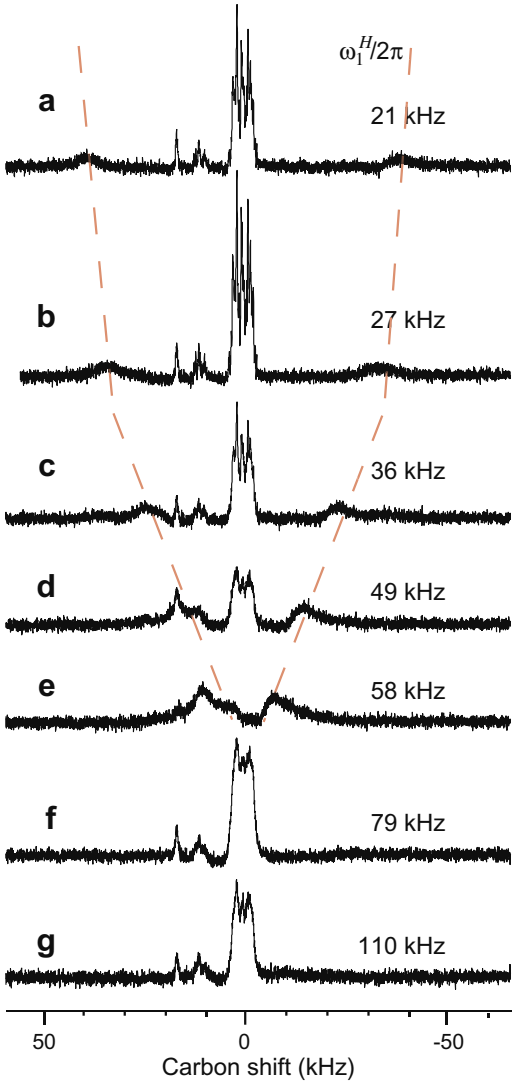

Fig. 6. CP/MAS carbon spectra of fully (^{15}N,^{13}C)-labeled, oxidized human SOD recorded at 60 kHz MAS under CW heteronuclear decoupling, with different values of the decoupling rf-field ω_1^H.

approaching rotary resonance, though they are observable even 40 kHz away from rotary resonances.

Finally, Fig. 7 illustrates an exciting perspective raised by these spin-dynamics properties at ultra-fast MAS. Since relaxation is considerably enhanced in paramagnetic systems (T_1 is less than about 100 ms for all the ^{1}H in SOD), the repetition rate of signal acquisition is most of the time limited by the duty cycle of the probe. Combined with the low power CP ($\omega_1^H = 5$ kHz) and low power rf irradiation during acquisition ($\omega_1^H = 15$ kHz), the short ^{1}H T_1s of oxidized SOD allow the repetition rate of the experiments to be shortened from 3 s to 500 ms, still respecting the duty cycle, thereby compensating for the sensitivity loss due to the small sample volume of a 1.3 mm rotor. The overall result here is that quite remarkably, the 2D RFDR (Radio-Frequency-driven Dipolar Recoupling) correlation spectrum shown in Fig. 7 could be acquired in about 24 h with about 1 mg of SOD sample.

5. Conclusion

We have demonstrated that the use of MAS at so-called ultra-fast spinning speeds in solid-state NMR experiments makes possible the use of "totally low power" experiments. This is notably a way to reduce the duty cycle of the probe and, above all, to dramat-

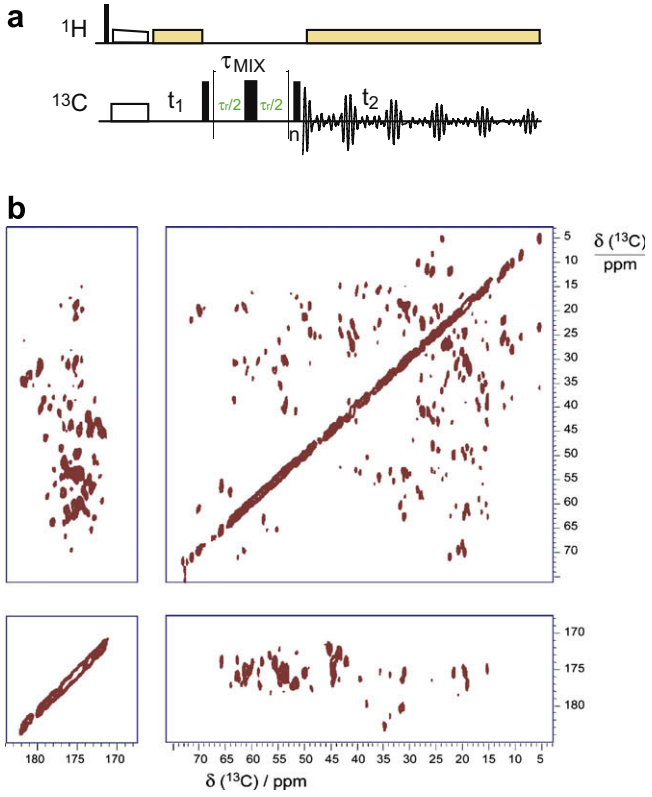

Fig. 7. ^{13}C–^{13}C RFDR pulse sequence (a) and the resulting spectrum (b) of the experiment performed on fully (^{15}N,^{13}C)-labeled, oxidized human SOD recorded at 60 kHz MAS (CP time 250 μs, ns = 280, t_1 increments = 600, $t_1^{MAX} = 5$ ms, $t_2^{MAX} = 20$ ms, total acquisition time = 25 h).

ically reduce unwanted heating which can lead to deterioration of the sample. Furthermore, provided that relaxation times are short enough, the recycling delay in the experiment can be reduced with a spectacular gain in overall sensitivity per unit time. Here this effect was demonstrated with a paramagnetic metalloprotein sample, ensuring short T_1s. However, paramagnetic doping could make similar experiments possible on diamagnetic samples [34]. We have also shown that because of interferences between MAS and decoupling, special care should be taken in the choice of the relative values of the decoupling and rotation frequencies. One can also observe rotational decoupling sidebands under ultra-fast MAS.

Acknowledgments

We acknowledge financial support from the CNRS Région Rhône-Alpes, the Ministére de la Recherche et l'Enseignement Supérieur, from the Access to research Infrastructures activity in the 6th Framework Program of the EC (Contract No. RII3-026145, EU-NMR), from the ANR jeunes chercheurs, jeunes chercheuses (2005), and from Ente Cassa di Risparmio di Firenze. NMR spectra were recorded at Bruker Biospin (Karlsruhe) and at the Rhone-Alpes Large Scale Facility for NMR (Lyon).

Appendix A. Quasi-equilibrium analysis of CP under MAS

Using quasi-equilibrium spin thermodynamics and following the formalism presented in [35], the maximum polarization achievable for ZQ- and DQCP under fast MAS can be predicted. The Hamiltonian giving rise to ZQCP at the Hartmann–Hahn matching condition of $\omega_1^I = \omega_1^S - p\omega_r$ is

$$\mathrm{H} = -\omega_1^S S_Z - (\omega_1^S - p\omega_r) I_Z + \omega_r R_{Z'} - \frac{1}{2}\omega_{IS}^{(p,0)}(I_+ S_{-p} + I_- S_+ F_p). \tag{A1}$$

This Hamiltonian implies that there are three energy reservoirs in the system: the *I*- and *S*-spin and rotation reservoirs. These reservoirs correspond to three mutually commuting parts of the Hamiltonian,

$$\begin{aligned} \mathrm{H}_1^0 &= -\omega_1^S S_Z \\ \mathrm{H}_2^0 &= -(\omega_1^S - p\omega_r) I_Z \\ \mathrm{H}_3^0 &= \omega_r R_{Z'}. \end{aligned} \tag{A2}$$

These three reservoirs are coupled together by the terms that lead to ZQCP,

$$V = -\frac{1}{2}\omega_{IS}^{(p,0)}(I_+ S_{-p} + I_- S_+ F_p) \tag{A3}$$

Quasi-invariants are operators that do not change the states connected by *V*. Two quasi-invariants can be formed in the case of ZQCP in an *IS* system:

$$Q_1 = \frac{1}{2}(p\omega_r - 2\omega_1^S)(I_Z + S_Z) \tag{A4}$$

and

$$Q_2 = \frac{1}{2}\omega_r(pI_Z - pS_Z + 2R_{Z'}). \tag{A5}$$

Projecting the initial spin-locked density matrix, $\sigma_{in} = \alpha_I I_Z$ where $\alpha_I = -\frac{\hbar\omega_0^I}{kT_L Tr[\mathbf{1}]}$ and I_Z is quantized along the rf-field, onto these quasi-invariants allows the quasi-equilibrium density matrix to be found. Using a superoperator formalism where for the operators *A* and *B*, $(A|B) = Tr\{AB\}$, the projection of the initial density matrix onto Q_1 is

$$\begin{aligned} \frac{(\sigma_{in}|Q_1)}{(Q_1|Q_1)}Q_1 &= \frac{Tr\{\alpha_I I_Z[\frac{1}{2}(p\omega_r - 2\omega_1^S)(I_Z + S_Z)]\}}{Tr\{[\frac{1}{2}(p\omega_r - 2\omega_1^S)(I_Z + S_Z)][\frac{1}{2}(p\omega_r - 2\omega_1^S)(I_Z + S_Z)]\}} \\ &\times \left[\frac{1}{2}(p\omega_r - 2\omega_1^S)(I_Z + S_Z)\right] = \frac{\frac{1}{2}\alpha_I(p\omega_r - 2\omega_1^S)[Tr\{I_Z^2\} + Tr\{I_Z S_Z\}]}{\frac{1}{4}[(p\omega_r - 2\omega_1^S)]^2 Tr\{[(I_Z + S_Z)(I_Z + S_Z)]\}} \\ &\times \left[\frac{1}{2}(p\omega_r - 2\omega_1^S)(I_Z + S_Z)\right]. \end{aligned} \tag{A6}$$

Canceling terms and using that $Tr\{I_Z^2\} = Tr\{S_Z^2\} = \frac{1}{2}$ and the orthogonality of I_Z and S_Z, $Tr\{I_Z S_Z\} = Tr\{S_Z I_Z\} = 0$, it is found that

$$\frac{(\sigma_{in}|Q_1)}{(Q_1|Q_1)}Q_1 = \frac{1}{2}\alpha_I(I_Z + S_Z). \tag{A7}$$

Similarly for the projection onto Q_2,

$$\begin{aligned} \frac{(\sigma_{in}|Q_2)}{(Q_2|Q_2)}Q_2 &= \frac{Tr\{\alpha_I I_Z[\frac{1}{2}\omega_r(pI_Z - pS_Z + 2R_{Z'})]\}}{Tr\{[\frac{1}{2}\omega_r(pI_Z - pS_Z + 2R_{Z'})][\frac{1}{2}\omega_r(pI_Z - pS_Z + 2R_{Z'})]\}} \\ &\times \left[\frac{1}{2}\omega_r(pI_Z - pS_Z + 2R_{Z'})\right] = \frac{\frac{1}{2}\omega_r\alpha_I\left[pTr\{I_Z^2\} - pTr\{I_Z S_Z\} + 2Tr\{I_Z R_{Z'}\}\right]}{\frac{1}{4}\omega_r^2 Tr\{(pI_Z - pS_Z + 2R_{Z'})(pI_Z - pS_Z + 2R_{Z'})\}} \\ &\times \left[\frac{1}{2}\omega_r(pI_Z - pS_Z + 2R_{Z'})\right]. \end{aligned} \tag{A8}$$

Again using the orthogonality of I_Z and S_Z as well as their orthogonality to $R_{Z'}$, $Tr\{I_Z R_{Z'}\} = Tr\{S_Z R_{Z'}\} = 0$ and canceling like terms, (A8) can be simplified to

$$\begin{aligned} \frac{(\sigma_{in}|Q_2)}{(Q_2|Q_2)}Q_2 &= \frac{p\alpha_I Tr\{I_Z^2\}}{p^2 Tr\{I_Z^2\} + p^2 Tr\{S_Z^2\} + 4Tr\{R_{Z'}^2\}}(pI_Z - pS_Z \\ &\quad + 2R_{Z'}) \\ &= \frac{\frac{1}{2}p\alpha_I}{p^2 + 4Tr\{R_{Z'}^2\}}(pI_Z - pS_Z + 2R_{Z'}). \end{aligned} \tag{A9}$$

Since the $Tr\{R_{Z'}^2\} = \infty$, Eq. (A9) becomes

$$\frac{(\sigma_{in}|Q_2)}{(Q_2|Q_2)}Q_2 = \frac{\frac{1}{2}p\alpha_I}{p^2+4(\infty)}(pI_Z - pS_Z + 2R_{Z'}) = 0. \tag{A10}$$

The quasi-equilibrium density matrix for ZQCP is

$$\sigma_{QE}^{ZQCP} = \frac{1}{2}\alpha_I(I_Z + S_Z). \tag{A11}$$

Thus the expectation value of S-spin magnetization after ZQCP is

$$\begin{aligned}\langle S_Z\rangle_{QE}^{ZQCP} &= Tr\{S_Z\sigma_{QE}^{ZQCP}\} = \frac{1}{2}\alpha_I(Tr\{S_ZI_Z\} + Tr\{S_Z^2\})\\ \langle S_Z\rangle_{QE}^{ZQCP} &= \frac{1}{4}\alpha_I.\end{aligned} \tag{A12}$$

The quasi-equilibrium transfer due to DQCP can be similarly calculated. In this case the three mutually commuting parts of the Hamiltonian and the coupling term are

$$\begin{aligned}H_1^0 &= -\omega_1^S S_Z\\ H_2^0 &= -(p\omega_r - \omega_1^S)I_Z\\ H_3^0 &= \omega_r R_{Z'}.\\ V &= -\frac{1}{2}\omega_{IS}^{(p,0)}(I_+S_+F_p + I_-S_-F_{-p}),\end{aligned} \tag{A13}$$

The two quasi-invariants that can be formed in the case of DQCP in an IS system are

$$Q_1 = \frac{1}{2}(2\omega_1^S - p\omega_r)(I_Z - S_Z) \tag{A14}$$

and

$$Q_2 = -\frac{1}{2}\omega_r(pI_Z + pS_Z - 2R_{Z'}). \tag{A15}$$

The projection of the initial density matrix onto Q_1 is

$$\frac{(\sigma_{in}|Q_1)}{(Q_1|Q_1)}Q_1 = \frac{1}{2}\alpha_I(I_Z - S_Z), \tag{A16}$$

while that onto Q_2,

$$\frac{(\sigma_{in}|Q_2)}{(Q_2|Q_2)}Q_2 = \frac{\frac{1}{2}p\alpha_I}{p^2+4Tr\{R_{Z'}^2\}}(pI_Z + pS_Z - 2R_{Z'}) = 0, \tag{A17}$$

since the $Tr\{R_{Z'}^2\} = \infty$. These results imply that the quasi-equilibrium density matrix for DQCP is

$$\sigma_{QE}^{DQCP} = \frac{1}{2}\alpha_I(I_Z - S_Z). \tag{A18}$$

Thus the expectation value of S-spin magnetization after DQCP is

$$\begin{aligned}\langle S_Z\rangle_{QE}^{DQCP} &= Tr\{S_Z\sigma_{QE}^{DQCP}\} = \frac{1}{2}\alpha_I(Tr\{S_ZI_Z\} - Tr\{S_Z^2\})\\ \langle S_Z\rangle_{QE}^{DQCP} &= -\frac{1}{4}\alpha_I.\end{aligned} \tag{A19}$$

Both ZQCP and DQCP lead to enhancement of the S-spin signal by an amount $\frac{1}{4}\alpha_I$; however, the sign of the enhancement is opposite for the two types of CP. Thus it is expected that the if the results of ZQCP are phased for positive peaks, DQCP will produce negatively phased peaks. This result can be seen by examining which energy levels have their population equalized by the CP process. In ZQCP, the populations of the $|M-1,\alpha\rangle$ and $|M,\beta\rangle$ states are equalized while the $|M-1,\beta\rangle$ and $|M,\alpha\rangle$ are unaffected. This leads to population difference for the S-spin transition of $\frac{1}{4}\alpha_I$. Similarly for DQCP the populations of the $|M-1,\beta\rangle$ and $|M,\alpha\rangle$ states are equalized while $|M-1,\alpha\rangle$ and $|M,\beta\rangle$ are unaffected, leading to population difference for the S-spin transition of $-\frac{1}{4}\alpha_I$. If the CP matching curve under ultra-fast MAS is measured, ZQCP is expected to give rise to a series of strong positively phased peaks spaced by $\pm p\omega_r$ about the normal Hartman–Hahn condition of $\omega_1^I = \omega_1^S$. In addition, strong, negatively phased peaks will appear at $\omega_1^I = p\omega_r - \omega_1^S$ due to DQCP.

References

[1] F. Castellani, B. van Rossum, A. Diehl, M. Schubert, K. Rehbein, H. Oschkinat, Structure of a protein determined by solid-state magic-angle-spinning NMR spectroscopy, Nature 420 (2002) 98–102.
[2] A.E. McDermott, Structural and dynamic studies of proteins by solid-state NMR spectroscopy: rapid movement forward, Curr. Opin. Struct. Biol. 14 (2004) 554–561.
[3] R. Tycko, Progress towards a molecular-level structural understanding of amyloid fibrils, Curr. Opin. Struct. Biol. 14 (2004) 96–103.
[4] M. Baldus, Solid-state NMR spectroscopy: molecular structure and organization at the atomic level, Angew. Chem. Int. Ed. 45 (2006) 1186–1188.
[5] A. Lange, K. Giller, S. Hornig, M.F. Martin-Eauclaire, O. Pongs, S. Becker, M. Baldus, Toxin-induced conformational changes in a potassium channel revealed by solid-state NMR, Nature 440 (2006) 959–962.
[6] C. Wasmer, A. Lange, H. Van Melckebeke, A.B. Siemer, R. Riek, B.H. Meier, Amyloid fibrils of the HET-s(218–289) prion form a beta solenoid with a triangular hydrophobic core, Science 319 (2008) 1523–1526.
[7] M. Ernst, M.A. Meier, T. Tuherm, A. Samoson, B.H. Meier, Low-power high-resolution solid-state NMR of peptides and proteins, J. Am. Chem. Soc. 126 (2004) 4764–4765.
[8] M. Ernst, A. Samoson, B.H. Meier, Low-power decoupling in fast magic-angle spinning NMR, Chem. Phys. Lett. 348 (2001) 293–302.
[9] Y. Ishii, N.P. Wickramasinghe, S. Chimon, A new approach in 1D and 2D C-13 high-resolution solid-state NMR spectroscopy of paramagnetic organometallic complexes by very fast magic-angle spinning, J. Am. Chem. Soc. 125 (2003) 3438–3439.
[10] G. Kervern, G. Pintacuda, Y. Zhang, E. Oldfield, C. Roukoss, E. Kuntz, E. Herdtweck, J.M. Basset, S. Cadars, A. Lesage, C. Copéret, L. Emsley, Solid-state NMR of a paramagnetic DIAD-FeII catalyst: sensitivity, resolution enhancement, and structure-based assignments, J. Am. Chem. Soc. 128 (2006) 13545–13552.
[11] G. Kervern, S. Steuernagel, F. Engelke, G. Pintacuda, L. Emsley, Absence of Curie relaxation in paramagnetic solids yields long 1H coherence lifetimes, J. Am. Chem. Soc. 129 (2007) 14118–14119.
[12] A. Kentgens, Geoderma 80 (1997) 271–306.
[13] Y. Ishii, R. Tycko, Sensitivity enhancement in solid state N-15 NMR by indirect detection with high-speed magic angle spinning, J. Magn. Reson. 142 (2000) 199–204.
[14] D.H. Zhou, G. Shah, M. Cormos, C. Mullen, D. Sandoz, C.M. Rienstra, Proton-detected solid-state NMR spectroscopy of fully protonated proteins at 40 kHz magic-angle spinning, J. Am. Chem. Soc. 129 (2007) 11791–11801.
[15] D.H. Zhou, J.J. Shea, A.J. Nieuwkoop, W.T. Franks, B.J. Wylie, C. Mullen, D. Sandoz, C.M. Rienstra, Solid-state protein-structure determination with proton-detected triple-resonance 3D magic-angle-spinning NMR spectroscopy, Angew. Chem. Int. Ed. Engl. 46 (2007) 8380–8383.
[16] M. Ernst, A. Samoson, B.H. Meier, Low-power XiX decoupling in MAS NMR experiments, J. Magn. Reson. 163 (2003) 332–339.
[17] M. Kotecha, N.P. Wickramasinghe, Y. Ishii, Efficient low-power heteronuclear decoupling in C-13 high-resolution solid-state NMR under fast magic angle spinning, Magn. Reson. Chem. 45 (2007) S221–S230.
[18] J.M. Griffin, C. Tripon, A. Samoson, C. Filip, S.P. Brown, Low-load rotor-synchronised Hahn-echo pulse train (RS-HEPT) H-1 decoupling in solid-state NMR: factors affecting MAS spin-echo dephasing times, Magn. Reson. Chem. 45 (2007) S198–S208.
[19] B.H. Meier, Cross polarization under fast magic angle spinning—thermodynamical considerations, Chem. Phys. Lett. 188 (1992) 201–207.
[20] D. Marks, S. Vega, A theory for cross-polarization NMR of nonspinning and spinning samples, J. Magn. Reson. A 118 (1996) 157–172.
[21] S. Ray, V. Ladizhansky, S. Vega, Simulation of CPMAS signals at high spinning speeds, J. Magn. Reson. 135 (1998) 427–434.
[22] J.R. Sachleben, S. Caldarelli, L. Emsley, The effect of spin decoupling on line shapes in solid-state nuclear magnetic resonance, J. Chem. Phys. 104 (1996) 2518–2528.
[23] J.R. Sachleben, J. Gaba, L. Emsley, Floquet–van Vleck analysis of heteronuclear spin decoupling in solids: the effect of spinning and decoupling sidebands on the spectrum, Solid State Nucl. Magn. Reson. 29 (2006) 30–51.
[24] R. Ramachandran, V.S. Bajaj, R.G. Griffin, Theory of heteronuclear decoupling in solid-state nuclear magnetic resonance using multipole–multimode Floquet theory, J. Chem. Phys. 122 (2005) 164503–164516.
[25] M. Ernst, A. Samoson, B.H. Meier, Decoupling and recoupling using continuous-wave irradiation in magic-angle-spinning solid-state NMR: a unified description using bimodal Floquet theory, J. Chem. Phys. 123 (2005).
[26] M. Leskes, R.S. Thakur, P.K. Madhu, N.D. Kurur, S. Vega, Bimodal Floquet description of heteronuclear dipolar decoupling in solid-state nuclear magnetic resonance, J. Chem. Phys. 127 (2007).
[27] G. Pintacuda, N. Giraud, R. Pierattelli, A. Böckmann, I. Bertini, L. Emsley, Solid-state NMR spectroscopy of a paramagnetic protein: assignment and study of human dimeric oxidized CuII–ZnII superoxide dismutase (SOD), Angew. Chem. Int. Ed. Engl. 46 (2007) 1079–1082.

[28] E.O. Stejskal, J. Schaefer, J.S. Waugh, Magic-angle spinning and polarization transfer in proton-enhanced NMR, J. Magn. Reson. 28 (1977) 105–112.
[29] F. Engelke, T. Kind, D. Michel, M. Pruski, B.C. Gerstein, A theoretical approach for the calculation of the Hartmann–Hahn matching under cross polarization and magic-angle spinning, J. Magn. Reson. 95 (1991) 286–298.
[30] M. Baldus, A.T. Petkova, J. Herzfeld, R.G. Griffin, Cross polarization in the tilted frame: assignment and spectral simplification in heteronuclear spin systems, Mol. Phys. 95 (1998) 1197–1207.
[31] T.G. Oas, R.G. Griffin, M.H. Levitt, Rotary resonance recoupling of dipolar interactions in solid-state nuclear magnetic resonance spectroscopy, J. Chem. Phys. 89 (1988) 692–695.
[32] N.C. Nielsen, H. Bildsoe, H.J. Jakobsen, M.H. Levitt, Double-quantum homonuclear rotary resonance: efficient dipolar recovery in magic-angle spinning nuclear magnetic resonance, J. Chem. Phys. 101 (1994) 1805–1812.
[33] G. De Paëpe, B. Elena, L. Emsley, Characterization of heteronuclear decoupling through proton spin dynamics in solid-state nuclear magnetic resonance spectroscopy, J. Chem. Phys. 121 (2004) 3165–3180.
[34] N.P. Wickramasinghe, M. Kotecha, A. Samoson, J. Past, Y. Ishii, Sensitivity enhancement in C-13 solid-state NMR of protein microcrystals by use of paramagnetic metal ions for optimizing H-1 T-1 relaxation, J. Magn. Reson. 184 (2007) 350–356.
[35] M.H. Levitt, D. Suter, R.R. Ernst, Spin dynamics and thermodynamics in solid-state NMR cross polarization, J. Chem. Phys. 84 (1986) 4243–4255.